DALTON
FULL PAPER

Mass spectrometry-directed synthesis of 'early–late' sulfide-bridged heterobimetallic complexes from the metalloligand $[Pt_2(PPh_3)_4(\mu\text{-}S)_2]$ and oxo compounds of vanadium(V), molybdenum(VI) and uranium(VI)

S.-W. Audi Fong,[a] Woon Teck Yap,[a] Jagadese J. Vittal,[a] William Henderson *[b] and T. S. Andy Hor *[a]

[a] *Department of Chemistry, National University of Singapore, 3 Science Drive 3, 117543, Singapore*
[b] *Department of Chemistry, University of Waikato, Private Bag 3105, Hamilton, New Zealand*

Received 3rd September 2001, Accepted 24th January 2002
First published as an Advance Article on the web 20th March 2002

The metalloligand $[Pt_2(PPh_3)_4(\mu\text{-}S)_2]$ has been found to react with the transition metal oxo compounds, ammonium metavanadate, sodium molybdate, and the actinide complex uranyl nitrate to give sulfide-bridged heterobimetallic complexes $[Pt_2(PPh_3)_4(\mu_3\text{-}S)_2VO(OMe)_2]^+$, $[Pt_2(PPh_3)_4(\mu_3\text{-}S)_2MoO_2(OMe)]^+$, and $[Pt_2(PPh_3)_4(\mu_3\text{-}S)_2UO_2(\eta^2\text{-}NO_3)_2]$, respectively. Electrospray mass spectrometry (ESMS) was used to probe the reactivity of $[Pt_2(PPh_3)_4(\mu\text{-}S)_2]$ and thus identify likely targets for isolation and characterization. ESMS has also been used to investigate fragmentation pathways of the new species. No bimetallic species were detected with hydrated $La(NO_3)_3$ or $Th(NO_3)_4$, or with the lanthanide shift reagent Eu(fod)$_3$ (fod = 6,6,7,7,8,8,8-heptafluoro-2,2-dimethyl-3,5-octanedionate). X-Ray crystal structure determinations have been carried out on $[Pt_2(PPh_3)_4(\mu_3\text{-}S)_2VO(OMe)_2]^+$, **2**, (as its hexafluorophosphate salt) and $[Pt_2(PPh_3)_4(\mu_3\text{-}S)_2UO_2(\eta^2\text{-}NO_3)_2]$, **4**. The vanadium atom of **2** has a distorted square pyramidal geometry, while the uranium in **4** has the expected linear dioxo coordination geometry, with two bidentate nitrates and a bidentate $\{Pt_2S_2\}$ moiety.

Introduction

The chemistry of heterometallic complexes containing widely divergent metal centers is of intense current interest. In particular, complexes supported by sulfide ligands have received much attention because of their relevance to biological systems and industrial catalysis.[1] The synthesis of early–late sulfide-bridged heterometallic compounds has been achieved by the use of suitable metalloligands;[2] a recent example is the synthesis of compounds with $\{TiM_2S_2\}$ cores (M = Rh, Ir) from $Cp_2Ti(SH)_2$.[3] The complex $[Pt_2(PPh_3)_4(\mu\text{-}S)_2]$, **1a**,[4] and closely related derivatives,[5] have been shown to be very useful metalloligands for the synthesis of a wide variety of homo- and heterometallic sulfide aggregates. However, attempts to synthesize mixed-metal complexes of **1a** with (chemically hard) early transition metals have not been successful prior to this work, with the exception of some low-valent derivatives of Mo, W, Mn, and Re.[6] Some derivatives with hard main group Lewis acids, *e.g.* In(III) and Ga(III), are also known.[7] Our current approach is to use electrospray ionization mass spectrometry (ESMS) to direct chemical syntheses. ESMS allows the identification of major and minor products in reaction solutions on a very small scale (thus minimizing wastage) and suggests targets for larger scale synthesis and full characterization. This combinatorial-type approach allows the screening of a wide range of different metal complexes; thus far, we have probed the chemistry of **1a**[8] and the related selenide analogue $[Pt_2(PPh_3)_4(\mu\text{-}Se)_2]$ **1b**[9] with a selection of chemically soft main group and late transition metal species. We have also recently reported the preliminary detection, using ESMS, of the species $[Pt_2(PPh_3)_4(\mu_3\text{-}S)_2VO(OMe)_2]^+$ from **1a** and V(O)(acac)$_2$.[8] This present paper describes the extension of this approach to the synthesis of sulfide-bridged aggregates with chemically hard oxo-metal species, including the isolation and structural characterization of the vanadyl and uranyl derivatives $[Pt_2(PPh_3)_4(\mu_3\text{-}S)_2VO(OMe)_2]^+$ and $[Pt_2(PPh_3)_4(\mu_3\text{-}S)_2UO_2(\eta^2\text{-}NO_3)_2]$, respectively.

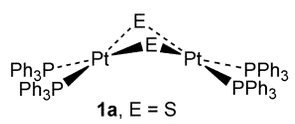

1a, E = S
1b, E = Se

Results and discussion

Reactivity survey using electrospray mass spectrometry

The reactions of complex **1a** with various anionic transition metal oxoanions (and thio-analogues for comparison) were initially probed by positive-ion ESMS; results are given in Table 1.

Reaction of **1a** with ammonium metavanadate $[NH_4VO_3]$ in methanol gave a clear, orange solution. The positive-ion electrospray (ES) mass spectrum (cone voltage 20 V) showed a single ion at *m*/*z* 1632, assigned to $[Pt_2(PPh_3)_4(\mu_3\text{-}S)_2VO(OMe)_2]^+$. This species remains stable up to a cone voltage of 100 V, whereupon fragmentation occurs by loss of PPh_3 and MeOH, with concomitant cyclometallation of a PPh_3 ligand, giving a species $[M - PPh_3 - MeOH]^+$ at *m*/*z* 1337. Loss of a second methanol gives an ion at *m*/*z* 1307. Further increasing the cone voltage to 110 V results in a new peak at *m*/*z* 1075 due to $[M - 2PPh_3 - MeOH]^+$, resulting from the loss of a second PPh_3 from $[M - PPh_3 - MeOH]^+$ (*m*/*z* 1337). The ES mass spectrum at 110 V is shown in Fig. 1, while the proposed fragmentation pathway is given in Scheme 1. A further 10 V increase in cone voltage removes another methanol, giving $[M - 2PPh_3 - 2MeOH]^+$ at *m*/*z* 1043. This species could be envisaged to contain two cyclometallated triphenylphosphines, *viz.* $[Pt_2(\eta^2\text{-}C_6H_4PPh_2\text{-}C^2,P)_2(\mu_3\text{-}S)_2VO]^+$. Further increasing the cone voltage did not lead to the loss of any further methanol fragment, supporting the initial assignment of the $[Pt_2(PPh_3)_4(\mu_3\text{-}S)_2VO(OMe)_2]^+$ ion. Consistent with this, the corresponding $[Pt_2(PPh_3)_4(\mu_3\text{-}S)_2VO(OEt)_2]^+$ ion (*m*/*z* 1660) was observed in ethanol solution. It is surprising to note the facile

 DOI: 10.1039/b107939p

Table 1 Species observed in the electrospray mass spectrometric analysis of **1a** with added transition metal complexes. (S–S) = complex **1a**

Mixture	Solvent	Cone voltage/V	Principal ions (*m*/*z*, %)
1a + NH_4VO_3	MeOH	20	$[(S–S)VO(OMe)_2]^+$ ($[M]^+$; 1632, 100)
		80	$[M]^+$ (1632, 100)
		100	$[M - PPh_3 - 2MeOH]^+$ (1307, 27), $[M - PPh_3 - MeOH]^+$ (1337, 63), $[M]^+$ (1632, 100)
		110	$[M - 2PPh_3 - MeOH]^+$ (1075, 7), $[M - PPh_3 - 2MeOH]^+$ (1307, 29), $[M - PPh_3 - MeOH]^+$ (1337, 100), $[M]^+$ (1632, 32)
		120	$[M - 2PPh_3 - 2MeOH]^+$ (1043, 4), $[M - 2PPh_3 - MeOH]^+$ (1075, 13), $[M - PPh_3 - 2MeOH]^+$ (1307, 23), $[M - PPh_3 - MeOH]^+$ (1337, 100), $[M]^+$ (1632, 13)
		140	$[M - 2PPh_3 - 2MeOH - PhH]^+$ (965, 13), $[M - 2PPh_3 - 2MeOH]^+$ (1043, 32), $[M - 2PPh_3 - MeOH]^+$ (1075, 53), $[M - PPh_3 - 2MeOH]^+$ (1307, 17), $[M - PPh_3 - MeOH]^+$ (1337, 100), $[M]^+$ (1632, 20)
		160	$[M - 2PPh_3 - 2MeOH - 3PhH]^+$ (809, 18), $[M - 2PPh_3 - 2MeOH - 2PhH]^+$ (887, 37), $[M - 2PPh_3 - 2MeOH - PhH]^+$ (965, 100), $[M - 2PPh_3 - 2MeOH]^+$ (1043, 82), $[M - 2PPh_3 - MeOH]^+$ (1075, 67), $[M - PPh_3 - 2MeOH]^+$ (1307, 9), $[M - PPh_3 - MeOH]^+$ (1337, 38), $[M]^+$ (1632, 51)
		180	$[M - 2PPh_3 - 2MeOH - 3PhH]^+$ (809, 72), $[M - 2PPh_3 - 2MeOH - 2PhH]^+$ (887, 85), $[M - 2PPh_3 - 2MeOH - PhH]^+$ (965, 100), $[M - 2PPh_3 - 2MeOH]^+$ (1043, 29), $[M - 2PPh_3 - MeOH]^+$ (1075, 15), $[M - PPh_3 - 2MeOH]^+$ (1307, 3), $[M - PPh_3 - MeOH]^+$ (1337, 10), $[M]^+$ (1632, 60)
	EtOH	20	$[(S–S)VO(OEt)_2]^+$ ($[M]^+$; 1660, 100)
1a + K_2CrO_4	MeOH	20	$[(S–S) + 2H]^{2+}$ (752, 100), $[(S–S) + 2H + Cl]^+$ (1538, 41)
1a + K_2MoO_4	MeOH	20	$[(S–S)MoO_2(OMe)]^+$ ($[M]^+$; 1663, 100)
		80	$[M]^+$ (1663, 100)
		100	$[M - PPh_3 - MeOH]^+$ (1369, 33), $[M]^+$ (1663, 100)
		120	$[Pt(PPh_3)(\eta^2\text{-}C_6H_4PPh_2)]^+$ (718, 13), $[M - PPh_3 - MeOH]^+$ (1369, 100), $[M]^+$ (1663, 30)
		140	$[Pt(PPh_3)(\eta^2\text{-}C_6H_4PPh_2)]^+$ (718, 68), $[Pt(PPh_3)(\eta^2\text{-}C_6H_4PPh_2) + MeOH]^+$ (750, 17), $[M - 2PPh_3 - MeOH - PhH]^+$ (1029, 16), unidentified (1089, 25), $[M - 2PPh_3 - MeOH]^+$ (1107, 28), $[M - PPh_3 - MeOH - PhH]^+$ (1291, 30), $[M - PPh_3 - MeOH]^+$ (1369, 100), $[M]^+$ (1663, 24), $[M + MeOH]^+$ (1695, 4)
		160	$[Pt(PPh_3)(\eta^2\text{-}C_6H_4PPh_2)]^+$ (718, 100), $[Pt(PPh_3)(\eta^2\text{-}C_6H_4PPh_2) + MeOH]^+$ (750, 26), $[M - 2PPh_3 - MeOH - PhH]^+$ (1029, 38), unidentified (1089, 27), $[M - 2PPh_3 - MeOH]^+$ (1107, 25), $[M - PPh_3 - MeOH - PhH]^+$ (1291, 30), $[M - PPh_3 - MeOH]^+$ (1369, 20), $[M]^+$ (1663, 31), $[M + MeOH]^+$ (1695, 3)
	EtOH	20	$[(S–S)MoO_2(OEt)]^+$ (1677, 100)
1a + Na_2WO_4	MeOH	20	$[(S–S) + 2H]^{2+}$ (752, 20), $[(S–S) + H]^+$ (1504, 100), $[(S–S) + 2H + Cl]^+$ (1538, 56)
1a + $KMnO_4$	MeOH	20	$[(S–S) + 2H]^{2+}$ (752, 100), $[(S–S) + H]^+$ (1504, 3)
1a + NH_4ReO_4	MeOH	20	$[(S–S) + 2H]^{2+}$ (752, 23), $[(S–S) + H]^+$ (1504, 100)

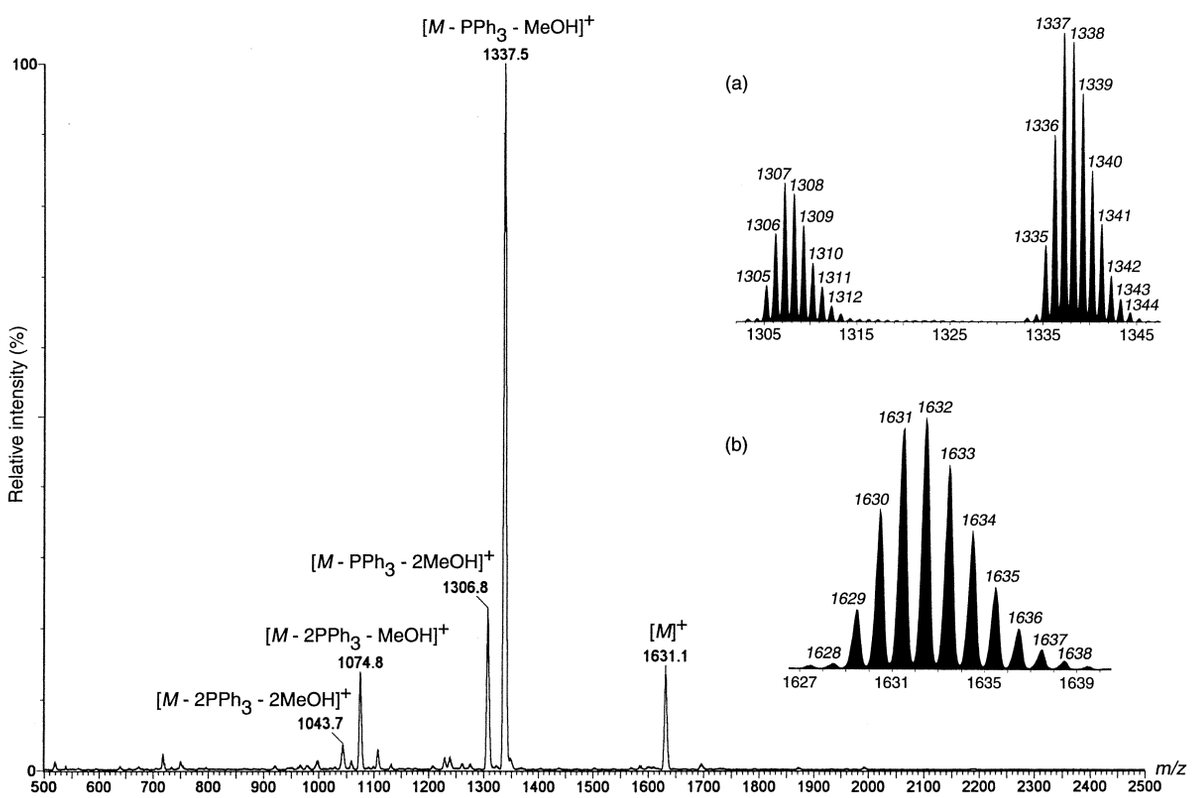

Fig. 1 Positive-ion electrospray mass spectrum of $[Pt_2(PPh_3)_4(\mu_3\text{-}S)_2VO(OMe)_2]^+$ ($[M]^+$) in methanol at a cone voltage of +110 V. The insets show the observed isotope distribution patterns for (a) the fragment ions $[M - PPh_3 - 2MeOH]^+$ (*m*/*z* 1307) and $[M - PPh_3 - MeOH]^+$ (*m*/*z* 1337) formed by cyclometallation of one or two PPh_3 ligands, and (b) the parent ion $[M]^+$ (*m*/*z* 1632) (refer to Scheme 1 for structures).

alcoholysis of the vanadium centre and the strong interaction of the hard V=O centre with the soft metalloligand **1a**. Presumably, the conversion of anionic vanadate into the cationic $V(O)(OR)_2^+$ species greatly increases its Lewis acidity towards the $\{Pt_2S_2\}$ moiety.

There was no detectable reaction between **1a** and K_2CrO_4. However, the facile reaction of **1a** with MoO_4^{2-} was in stark contrast, giving a solitary ion at *m*/*z* 1663 in the ES spectrum at 20 V, due to $[Pt_2(PPh_3)_4(\mu_3\text{-}S)_2MoO_2(OMe)]^+$, with the corresponding ethoxy analogue (*m*/*z* 1677) observed in ethanol. This

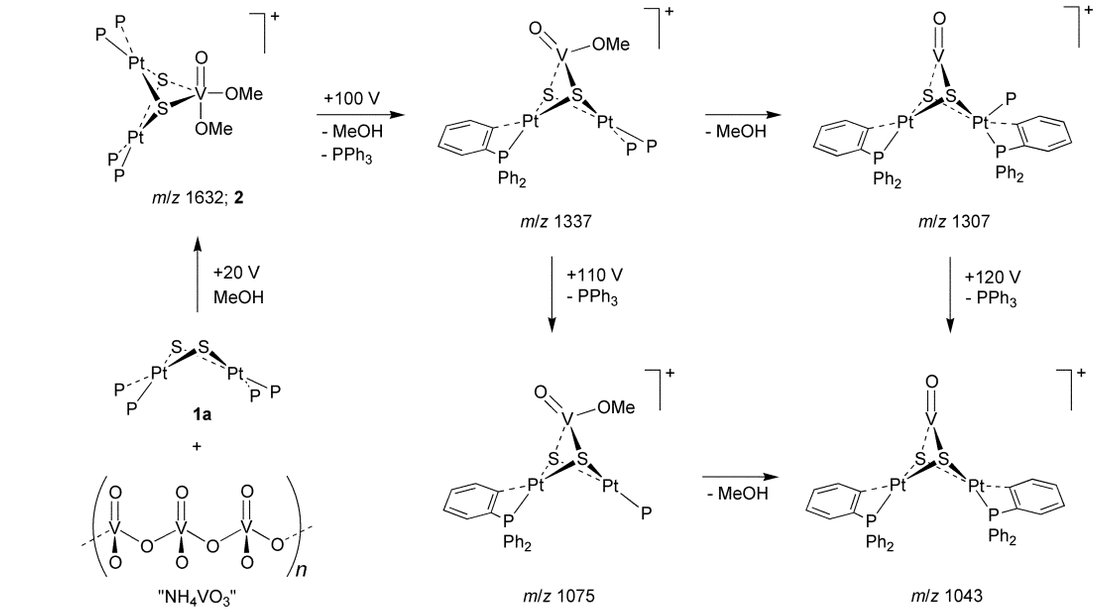

Scheme 1 Fragmentation pathway for $[Pt_2(PPh_3)_4(\mu_3\text{-}S)_2VO(OMe)_2]^+$ in the positive-ion electrospray mass spectrum. P = PPh_3.

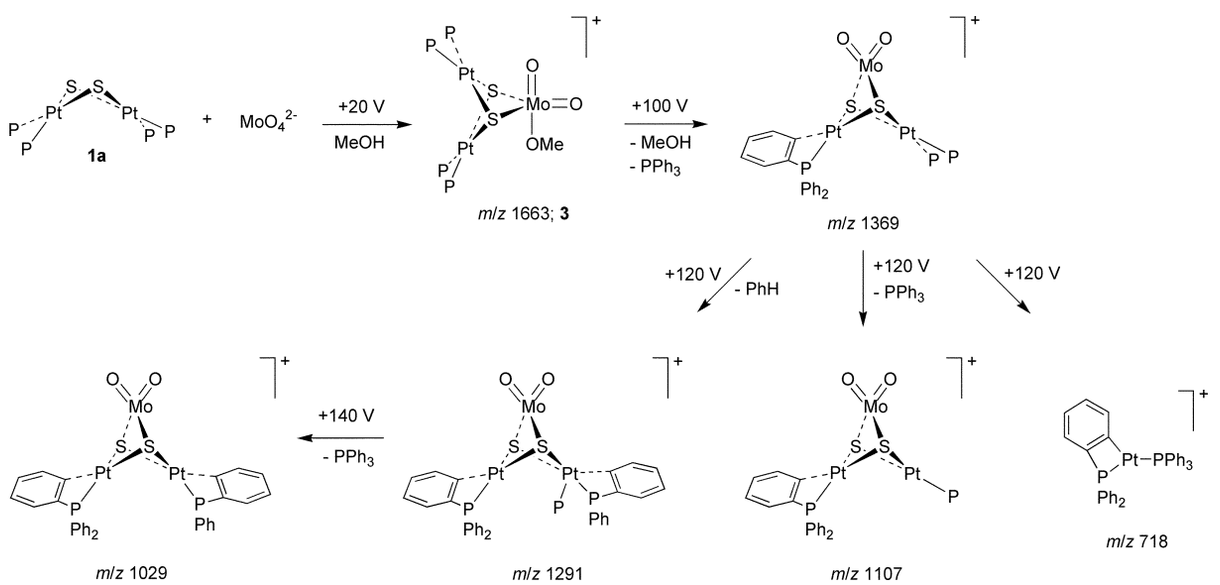

Scheme 2 Fragmentation pathway for $[Pt_2(PPh_3)_4(\mu_3\text{-}S)_2MoO_2(OMe)]^+$ in the positive-ion electrospray mass spectrum. P = PPh_3.

reactivity, which parallels the reactivity with vanadate ions earlier, is consistent with the fact that MoS_4^{2-} (and WS_4^{2-}) are well known, but CrS_4^{2-} does not exist. The fragmentation pathway (Scheme 2) reveals that the ion $[Pt_2(PPh_3)_4(\mu_3\text{-}S)_2MoO_2(OMe)]^+$ is stable up to a cone voltage of 80 V. At a cone voltage of 100 V, $[Pt_2(PPh_3)_4(\mu_3\text{-}S)_2MoO_2(OMe)]^+$ begins to undergo concomitant loss of PPh_3 and MeOH (through cyclometallation of a PPh_3 ligand) giving $[M - PPh_3 - MeOH]^+$ (*m*/*z* 1369). Upon further increasing the cone voltage to 120 V and above, species such as $[Pt(PPh_3)(\eta^2\text{-}C_6H_4PPh_2\text{-}C^2,P)]^+$ (*m*/*z* 718), $[M - 2PPh_3 - MeOH - PhH]^+$ (*m*/*z* 1029), $[M - 2PPh_3 - MeOH]^+$ (*m*/*z* 1107), and $[M - PPh_3 - MeOH - PhH]^+$ (*m*/*z* 1291) appear. It is also noteworthy that throughout this cone voltage-induced fragmentation, only one MeOH is lost from the parent cation. The ion $[Pt(PPh_3)(\eta^2\text{-}C_6H_4PPh_2\text{-}C^2,P)]^+$ (*m*/*z* 718) is commonly observed when platinum triphenylphosphine complexes are subjected to high cone voltages.[10] Surprisingly, no reaction was observed between **1a** and WO_4^{2-}.

The reaction of **1a** with $UO_2(NO_3)_2{\cdot}6H_2O$ gave $[Pt_2(PPh_3)_4(\mu_3\text{-}S)_2UO_2(NO_3)(MeOH)]^+$ (*m*/*z* 1867) and $[Pt_2(PPh_3)_4(\mu_3\text{-}S)_2UO_2(MeOH)_2]^{2+}$ (*m*/*z* 918.5). However, reaction of **1a** with hydrated $La(NO_3)_3{\cdot}6H_2O$, $Eu(fod)_3$ (fod = 6,6,7,7,8,8,8-heptafluoro-2,2-dimethyl-3,5-octanedionate), or $Th(NO_3)_4{\cdot}6H_2O$ resulted in the detection of only $[\mathbf{1a} + H]^+$ (*m*/*z* 1504) and $[\mathbf{1a} + 2H]^{2+}$ (*m*/*z* 752) ions. Similarly, both $KMnO_4$ and NH_4ReO_4 gave no observable reaction with **1a**.

This survey, probing reactivity on a small scale using electrospray mass spectrometry, clearly indicates the power of this approach in identifying suitable and unsuitable substrates for further study on the macroscopic scale, described in the next section.

Syntheses

The observation of the novel vanadium-, molybdenum-, and uranium-containing cations provided the impetus to carry out macroscopic syntheses. Reaction of **1a** with 2 equivalents of NH_4VO_3 in MeOH, followed by metathesis with excess NH_4PF_6, gave $[Pt_2(PPh_3)_4(\mu_3\text{-}S)_2VO(OMe)_2][PF_6]$, **2**, isolated as orange–red microcrystals in 72% yield. In a similar fashion, $[Pt_2(PPh_3)_4(\mu_3\text{-}S)_2MoO(OMe)_2][PF_6]$, **3**, was obtained as a red solid in 68% yield from **1a** and Na_2MoO_4. The reaction between **1a** and $UO_2(NO_3)_2{\cdot}6H_2O$ gave the uranyl nitrate adduct $[Pt_2(PPh_3)_4(\mu_3\text{-}S)_2UO_2(\eta^2\text{-}NO_3)_2]$, **4**, in 54% yield as a purple solid which is poorly soluble in methanol, but soluble in dichloromethane and chloroform. All complexes gave good elemental microanalytical data. Complexes **2** and **4** are the

first containing the Pt–S–V(O) and Pt–S–U linkages, though complexes with the $\{PtV_2S_2\}$ core are known.[11] The Pt–S–Mo linkage is also well known, occuring in complexes such as $[S_2Mo(\mu\text{-}S)_2Pt(PPh_3)_2]$.[12]

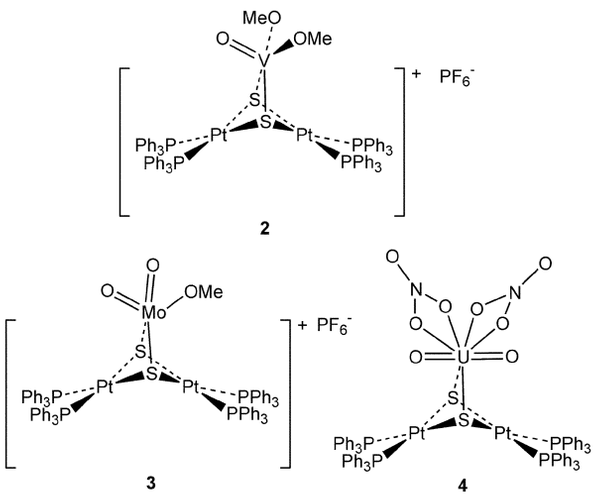

Complexes **2**–**4** are stable towards chlorinated solvents (such as dichloromethane and chloroform), allowing crystallization from these solvents. This is in marked contrast to the parent complex **1a**, which is known to react rapidly with chlorinated solvents.[4] Furthermore, a purple dichloromethane solution of **4** retains its purple colour when tri-*n*-octylphosphine oxide (a well-known ligand used in the solvent extraction of uranyl ions)[13] is added. These observations indicate a reasonably strong interaction between the $\{Pt_2S_2\}$ core and the uranyl moiety.

Crystal structure determinations

The molecular structure of **2** (Fig. 2) shows a triangular VPt_2 core capped on both sides by symmetrical μ_3-sulfido ligands (selected bond lengths and angles are reported in Table 2). There are two independent cations in the unit cell, and both show broadly similar structural features. The subsequent discussion is based around one of these ions. Neglecting the metal ··· metal interactions, the d^8 platinum(II) centers exhibit square-planar coordination environments, while the vanadium centre has a distorted square pyramidal geometry, with the vanadyl oxygen O(1) occupying the apical position. The V(1)–S(1)–S(2)–O(2)–O(3) plane deviates slightly from planarity by 0.176 Å (0.180 Å for the other independent ion). No significant d^0–d^8 bonding interactions are present [V(1) ··· Pt(1) 3.219(3), V(1) ··· Pt(2) 3.188(3) Å] and the Pt(1) ··· Pt(2) distance of 3.317(2) Å lies beyond the expected range for a Pt–Pt bond. This value compares favourably with those of other later transition metal and main group heterometallic aggregates of **1a**, *e.g.* $[Pt_2(PPh_3)_4(\mu\text{-}S)_2Ag(PPh_3)]^+$ [3.351(2) Å][14] and $[Pt_2(PPh_3)_4(\mu\text{-}S)_2Tl]^+$ [3.293(2) Å].[15] The dihedral angle of the $\{Pt_2S_2\}$ butterfly of ion 1 along the S(1) ··· S(2) axis is 130.4(6)°, with the two μ-sulfides chelated to the V atom at an angle of 73.47(14)°; these values compare well with those of related species.[4] The V(1)–O(1) bond length [1.618(13) Å] is similar to those of other vanadyl species with S_2O_2 donor sets, *e.g.* [V(O)(2-mercaptophenolate)$_2$]$^{2-}$, **5**, [1.611(5) Å],[16] while the V–OCH_3 bonds [1.818(12) and 1.749(13) Å] are shorter and the V–S bonds [2.457(4) and 2.476(5) Å] are longer than in **5** [average V–O 1.959(3), V–S 2.366(3) Å]. As can be seen in Fig. 2, there is a *pseudo* plane of symmetry passing through the two Pt atoms and the V=O group. The solid-state structure appears to be retained in solution, with two PPh_3 resonances observed in the ^{31}P NMR spectrum of the complex.

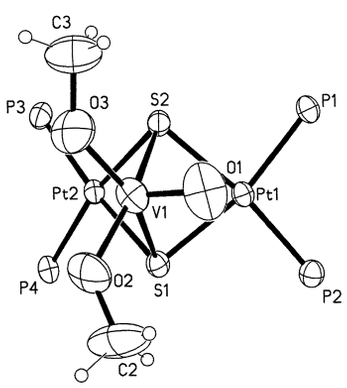

Fig. 2 Molecular structure of one of the crystallographically independent cations of $[Pt_2(PPh_3)_4(\mu_3\text{-}S)_2VO(OMe)_2][PF_6]$, **2**, with thermal ellipsoids at the 50% probability level. Phenyl rings have been omitted for clarity.

Table 2 Selected bond lengths (Å) and angles (°) for one of the crystallographically independent cations of $[Pt_2(PPh_3)_4(\mu_3\text{-}S)_2VO(OMe)_2][PF_6]$, **2**

Bond lengths			
Pt(1)–S(1)	2.350(4)	Pt(1)–S(2)	2.349(4)
Pt(1)–P(1)	2.307(4)	Pt(1)–P(2)	2.295(4)
Pt(2)–S(1)	2.354(4)	Pt(2)–S(2)	2.337(4)
Pt(2)–P(3)	2.277(4)	Pt(2)–P(4)	2.302(4)
V(1)–S(1)	2.457(4)	V(1)–S(2)	2.476(5)
V(1)–O(1)	1.618(13)	V(1)–O(2)	1.818(12)
V(1)–O(3)	1.749(13)	O(2)–C(2)	1.43(2)
O(3)–C(3)	1.44(2)		
Non-bonded distances			
Pt(1) ··· Pt(2)	3.317(2)	Pt(1) ··· V(1)	3.220(3)
Pt(2) ··· V(1)	3.188(3)		
Bond angles			
S(1)–Pt(1)–S(2)	77.78(13)	S(1)–Pt(2)–S(2)	77.96(13)
S(1)–V(1)–S(2)	73.47(14)	Pt(1)–S(1)–Pt(2)	89.67(12)
Pt(1)–S(1)–V(1)	84.06(13)	Pt(2)–S(1)–V(1)	82.96(13)
Pt(1)–S(2)–Pt(2)	90.12(13)	Pt(1)–S(2)–V(1)	83.66(14)
Pt(2)–S(2)–V(1)	82.91(13)		

The formulation of the uranyl nitrate complex **4** was also confirmed by an X-ray structure determination (selected bond lengths and angles are reported in Table 3). The molecular structure (Fig. 3) shows an eight-coordinate uranium central atom chelated by two bidentate nitrate ligands and simultaneously chelated by the $\{Pt_2S_2\}$ moiety, giving the usual hexagonal bipyramidal coordination geometry. The U–O(uranyl) bond lengths U(1)–O(1) and U(1)–O(2) [1.745(4) and 1.742(4) Å, respectively] are, as expected, considerably shorter than bonds to the nitrate oxygens [2.497(5)–2.513(5) Å]. The O(1)–U–O(2) bond angle of 174.74(19) Å reflects the steric bulk of the $Pt_2S_2(PPh_3)_4$ moiety, resulting in the uranyl oxygens bending away to relieve steric congestion. The dihedral angle of the $\{Pt_2S_2\}$ moiety, defined by the angle between the two platinum coordination planes, is 129.6°, which compares favourably with

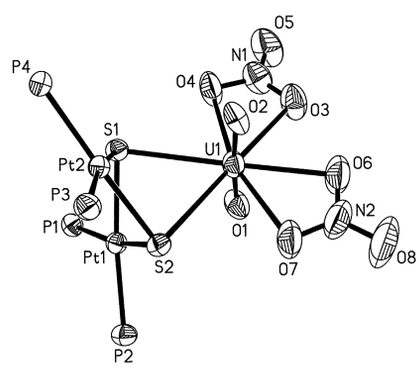

Fig. 3 Molecular structure of the cation of $[Pt_2(PPh_3)_4(\mu_3\text{-}S)_2UO_2(\eta^2\text{-}NO_3)_2]$, **4**, with thermal ellipsoids at the 50% probability level. Phenyl rings have been omitted for clarity.

Table 3 Selected bond lengths (Å) and angles (°) for $[Pt_2(PPh_3)_4(\mu_3\text{-}S)_2UO_2(\eta^2\text{-}NO_3)_2]$, **4**

Bond lengths			
Pt(1)–P(2)	2.2842(17)	Pt(1)–P(1)	2.3128(17)
Pt(2)–P(4)	2.2727(18)	Pt(2)–P(3)	2.3029(16)
Pt(1)–S(1)	2.3354(15)	Pt(1)–S(2)	2.3406(15)
Pt(2)–S(1)	2.3327(15)	Pt(2)–S(2)	2.3384(16)
U(1)–O(2)	1.742(4)	U(1)–O(1)	1.645(4)
U(1)–O(3)	2.502(4)	U(1)–O(4)	2.507(5)
U(1)–O(6)	2.513(5)	U(1)–O(7)	2.497(5)
N(1)–O(3)	1.253(7)	N(1)–O(4)	1.266(7)
N(1)–O(5)	1.215(6)	N(2)–O(6)	1.254(7)
N(2)–O(7)	1.243(8)	N(2)–O(8)	1.226(8)
U(1)–S(2)	2.8693(15)	U(1)–S(1)	2.8774(17)
Non-bonded distances			
U(1) ··· N(2)	2.929(8)	U(1) ··· N(1)	2.936(6)
U(1) ··· Pt(1)	3.5589(4)	U(1) ··· Pt(2)	3.6368(4)
Pt(1) ··· Pt(2)	2.2842(17)		
Bond angles			
O(2)–U(1)–O(1)	174.74(19)	S(2)–U(1)–S(1)	62.15(4)
O(2)–U(1)–S(2)	92.97(13)	O(1)–U(1)–S(2)	91.54(13)
O(2)–U(1)–S(1)	92.48(15)	O(1)–U(1)–S(1)	92.01(15)
O(3)–U(1)–O(4)	50.34(15)	O(7)–U(1)–O(6)	50.08(16)
P(2)–Pt(1)–P(1)	99.79(6)	P(4)–Pt(2)–P(3)	99.94(6)
S(1)–Pt(1)–S(2)	78.74(5)	S(1)–Pt(2)–S(2)	78.84(5)
Pt(2)–S(1)–Pt(1)	89.86(5)	Pt(2)–S(1)–U(1)	87.89(5)
Pt(1)–S(1)–U(1)	85.44(5)	Pt(2)–S(2)–Pt(1)	89.59(5)
Pt(2)–S(2)–U(1)	87.97(5)	Pt(1)–S(2)–U(1)	85.54(4)
O(5)–N(1)–O(3)	121.8(7)	O(5)–N(1)–O(4)	122.8(7)
O(3)–N(1)–O(4)	115.5(6)	O(8)–N(2)–O(7)	122.7(8)
O(8)–N(2)–O(6)	121.0(8)	O(7)–N(2)–O(6)	116.2(7)

other metal aggregates of the Pt_2S_2 core.[4] The small S(1)–U(1)–S(2) bite angle of 62.15(4) Å is a consequence of the coordination of the $\{Pt_2S_2\}$ moiety in the uranyl equatorial coordination plane; this angle is the smallest yet reported for a metal adduct of the $\{Pt_2S_2\}$ core, with values typically around 75–85°, depending on the coordination geometry of the metal centre.[4]

To our knowledge, few examples of heterometallic Pt–U compounds have been reported in the literature, and none containing Pt–S–U linkages. Two examples of M–U compounds (M = platinum group metal) are the palladium diethydithiocarbamate complex $[\{(Et_2NS_2)Pd(PPh_2O)_2\}_2UO_2(H_2O)]$, which has the uranyl moiety coordinated to the two Pd centres through the four bridging oxygens of the diphenylphosphinito ligands,[17] and the amidate-bridged complex $[(Ph_3P)_2Pt\{NC(O)CH_2CH_2\}_2]\cdot UO_3(NO_3)_2$, in which the two amide CO groups of the platinum complex coordinate to the uranyl moiety.[18] Other (non sulfide-bridged) platinum–uranium bimetallic compounds are known.[19] Complex **4** is the first structure of a uranyl nitrate complex with two sulfur donor ligands, though other uranyl complexes containing anionic ligands, such as dithiocarbamate or dithiophosphinate, are known, *e.g.* $[UO_2(S_2P^iPr)_2(H_2O)]$,[20] where the U–S bond distances (range 2.830–2.853 Å) are slightly shorter than in **4**, reflecting the anionic nature of the dithiophosphinate ligands.

Conclusions

This ESMS-assisted work has afforded useful insights towards the directed synthesis and isolation of heterometallic complexes that involve the $\{Pt_2S_2\}$ core and hard, oxophilic metal centers, in this case vanadium, molybdenum, and uranium. In principle, this could be extended to include other hard metal centers, including other actinides. The selectivity for complexation with uranium, but not thorium or lanthanum, is particularly noteworthy. This underscores the unparalleled utility of the $\{Pt_2S_2\}$ core as a powerful precursor to a wide array of heterometallic complexes, and opens an exciting new window of potential applications for $\{Pt_2S_2\}$ complexes.

Experimental

General

General experimental techniques were as described previously.[8,9] Reactions were carried out as under argon as a precautionary measure, though it is not strictly necessary; for example, a comparable yield of the uranyl complex **4** was obtained when the synthesis was carried out in air. $[Pt_2(PPh_3)_4(\mu\text{-}S)_2]$, **1a**, was prepared by the literature procedure.[21] Ammonium metavanadate, sodium molybdate, and uranyl nitrate hexahydrate were used as supplied by BDH.

Mass spectra were recorded in the positive-ion mode using a VG Platform II mass spectrometer. MeOH was used as the mobile phase, unless otherwise stated, because of the solubility of the ionic species formed in this solvent. The spectrometer employed a quadrupole mass filter with an *m*/*z* range 0–3000. The compounds were dissolved in the mobile phase to give a solution typically of approximate concentration 0.1 mmol L^{-1}, and spectra were recorded for freshly prepared solutions. The dilute sample solution was injected into the spectrometer *via* a Rheodyne injector fitted with a 10 μL sample loop. A Thermo Separation Products Spectra System P1000 LC pump delivered the solution to the mass spectrometer source (maintained at 60 °C) at a flow rate of 0.02 mL min^{-1}, and nitrogen was employed as both the drying and nebulising gas. Cone voltages were varied from +20 to +180 V in order to investigate the effect of higher cone voltages on the fragmentation of selected intact gas-phase ions. Theoretical isotope distributions, obtained using the ISOTOPE program,[22] were compared with experimental patterns to confirm ion assignment.

Syntheses

$[Pt_2(PPh_3)_4(\mu_3\text{-}S)_2VO(OMe)_2][PF_6]$, 2. Solid NH_4VO_3 (7.6 mg, 0.0650 mmol, excess) was added under argon to $[Pt_2(PPh_3)_4(\mu\text{-}S)_2]$, **1a**, (80.0 mg, 0.0532 mmol) in MeOH (20 mL) in a 100 mL Schlenk tube. The contents were stirred at 25 °C, initially giving an orange suspension which turned clear bright red after stirring overnight. The mixture was allowed to stir for an additional 24 h, giving a clear, intensely red solution. The solution was filtered through Celite; the filter cake and Celite were washed with MeOH (2 × 5 mL) until the washings were colorless. The pale orange washings and filtrate were combined (30 mL), and excess solid NH_4PF_6 (15 mg, 0.0920 mmol) added. After stirring for a further 2 h, a red solid precipitated. Distilled water (10 mL) was then added to the mixture to induce complete precipitation. The red solid was collected on a fine glass frit, washed successively with distilled water (2 × 10 mL), ethanol (5 mL), ether (10 mL), and dried *in vacuo*, giving red microcrystals of **2** (68.4 mg, 72%). Found: C, 49.75; H, 3.78; P, 8.67; S, 3.59; $C_{74}H_{66}F_6O_3P_5Pt_2S_2V$ requires C, 50.00; H, 3.74; P, 8.71; S, 3.61%. $^{31}P\text{-}\{^1H\}$ NMR (CD_3CN): δ_P 20.44 (t, $^1J_{Pt-P}$ = 3227, 2 PPh_3), 19.87 (t, $^1J_{Pt-P}$ = 3216, 2 PPh_3), −142.89 (septet, $^1J_{P-F}$ = 706 Hz, PF_6^-). ^1H NMR (CD_3CN): δ_H 3.29 (s, 6 H, 2 OCH_3), 7.55–7.01 (m, 60 H, 12 C_6H_5).

$[Pt_2(PPh_3)_4(\mu_3\text{-}S)_2MoO_2(OMe)][PF_6]$, 3. Following an analogous procedure to that for complex **2**, Na_2MoO_4 (7.6 mg, 0.0650 mmol, excess) was added to **1a** (80.0 mg, 0.0532 mmol) in MeOH (20 mL), initially giving an orange suspension which turned clear yellow after stirring overnight, and intensely red after stirring for an additional 24 h. Workup gave **3** as a red powder (58.9 mg, 68%). Found: C, 48.46; H, 3.54; P, 8.51; S, 3.52; $C_{73}H_{63}F_6MoO_3P_5Pt_2S_2$ requires C, 48.51; H, 3.51; P, 8.57; S, 3.55%. $^{31}P\text{-}\{^1H\}$ NMR ($CDCl_3$): δ_P 18.87 (t, $^1J_{Pt-P}$ = 3197, 4 PPh_3), −144.05 (septet, $^1J_{P-F}$ = 709 Hz, PF_6^-). ^1H NMR ($CDCl_3$): δ_H 3.49 (s, 3 H, OCH_3), 7.39–7.12 (m, 60 H, 12 C_6H_5).

$[Pt_2(PPh_3)_4(\mu_3\text{-}S)_2UO_2(\eta^2\text{-}NO_3)_2]$, 4. Solid $[UO_2(NO_3)_2\cdot 6H_2O]$ (26.1 mg, 0.0519 mmol) was added to an orange suspension of **1a** (78.0 mg, 0.0519 mmol) in MeOH (20 mL) in a

100 mL Schlenk tube containing a stir bar. The contents were stirred under argon, initially giving an orange suspension that turned clear purple after stirring for *ca.* 4 h. The mixture was allowed to stir for an additional 24 h, giving a violet suspension. The solid was collected on a fine glass frit, washed successively with water (2 × 10 mL), ethanol (5 mL), ether (10 mL), and dried *in vacuo*, giving **4** as a purple powder (52.6 mg, 54%). Found: C, 45.80; H, 3.20; P, 6.60; S, 3.40; $C_{72}H_{60}N_2O_8P_4Pt_2S_2U$ requires: C, 45.58; H, 3.19; P, 6.53; S, 3.38%. ^{31}P-{^1H} NMR ($CDCl_3$): δ_P 21.82 ($^1J_{Pt-P}$ = 3079 Hz; 4 PPh_3). ^1H NMR ($CDCl_3$): δ_H 6.95–7.44 (m, 60 H, 12 C_6H_5).

Crystallography

X-Ray structure of $[Pt_2(PPh_3)_4(\mu_3\text{-}S)_2VO(OMe)_2][PF_6]\cdot 0.5H_2O$, 2. Red single crystals of **2** were grown by slow evaporation of a methanol solution in a refrigerator at 5 °C; a red needle (0.20 mm × 0.18 mm × 0.10 mm) was selected and mounted. A total of 69229 reflections were collected ($-21 \geq h \leq 16$, $-49 \leq k \leq 39$, $-23 \leq l \leq 19$) in the θ range 1.80–25.00°, of which 24869 were independent (R_{int} = 0.0787), at 293(2) K using a Bruker AXS SMART CCD diffractometer. The structure was solved by direct methods (SHELXL-97)[23] in conjunction with standard difference Fourier techniques. For the monoclinic space group $P2_1/n$, there are two independent molecules in the unit cell. Soft constraints were applied to two PF_6 anions to maintain the octahedral geometry. The carbon atoms of several phenyl rings show high thermal activity. Refinement of anisotropic thermal parameters was not possible for the phenyl rings with subscripts F, H, I, L, V, W, and X. Attempts to resolve the disorder in these phenyl rings were futile and, hence, they were treated as regular hexagons in the least-squares cycles. The phenyl rings with subscripts V and W (bonded to P7) show close interactions [H(6V) ··· H(6W), 1.745 Å]. Such interactions can be explained only by invoking disorder in the orientations of the phenyl rings. Since neither the anisotropic thermal parameters could be refined nor reasonable disorder models could be achieved for these phenyl rings, we conclude that the disorders are diffusional in nature (thermal whizzing). Despite the poor quality data and disorder, the structural connectivity is proved beyond any doubt in **2**. The largest peak and hole in the difference map were 5.827 and −2.043 e Å^{-3}, respectively. The least-squares refinement converged normally, with residuals of R (based on F) = 0.0801, wR (based on F^2) = 0.1856, and GOF = 1.067 [based upon $I > 2\sigma(I)$].

Crystal data for $C_{74}H_{66}F_6O_3P_5Pt_2S_2V$: monoclinic, space group = $P2_1/n$, Z = 8, a = 17.7574(4), b = 41.8464(9), c = 19.3758(4) Å, β = 92.614(1)°, V = 14382.8(5) Å^3, ρ_{calc} = 1.642 g cm^{-3}, $F(000)$ = 6992, μ(Mo-Kα) = 4.239 mm^{-1}.

CCDC reference number 144506.

X-Ray structure of $[Pt_2(PPh_3)_4(\mu_3\text{-}S)_2UO_2(\eta^2\text{-}NO_3)_2]$, 4. Deep purple single crystals of **4** were grown by vapour diffusion of diethyl ether into a dichloromethane solution of the complex in a refrigerator at 5 °C; a purple block (0.18 mm × 0.13 mm × 0.13 mm) was selected and quickly mounted on a glass fibre using wax. A total of 39879 reflections were collected ($-26 \leq h \leq 26$, $-16 \leq k \leq 15$, $-27 \leq l \leq 28$) in the θ range 1.74–25.00°, of which 12198 were independent (R_{int} = 0.0659), at 296(2) K. Data were corrected for absorption using SADABS:[24] T_{max} and T_{min} 0.5454 and 0.4493, respectively. The structure was solved by direct methods in conjunction with standard difference Fourier techniques. Non-hydrogen atoms were refined anisotropically. Hydrogen atoms were placed in calculated (d_{C-H} = 0.96 Å) positions. The largest peak and hole in the difference map were 1.306 and −1.422 e Å^{-3}, respectively. The least-squares refinement converged normally, with final R indices [$I > 2\sigma(I)$] R_1 = 0.0352, wR_2 = 0.0457, and GOF = 0.857.

Crystal data for $C_{72}H_{60}N_2O_8P_4Pt_2S_2U$: monoclinic, space group = $P2_1/c$, Z = 4, a = 22.5463(9), b = 14.2378(6), c = 23.8747(10) Å, β = 115.291(1), V = 6929.4(5) Å^3, ρ_{calc} = 1.819 g cm^{-3}, $F(000)$ = 3640, μ(Mo-Kα) = 6.567 mm^{-1}.

CCDC reference number 169981.

See http://www.rsc.org/suppdata/dt/b1/b107939p/ for crystallographic data in CIF or other electronic format.

Acknowledgements

We thank the National University of Singapore (grant no. RP 960664/A) and the University of Waikato for financial support of this work, and Johnson Matthey plc for a generous loan of platinum. S.-W. A. F. is especially grateful to the NUS for a research scholarship and a visiting scholarship to visit Waikato University (grant no. RP 982755). We are grateful to Professor B. K. Nicholson (Waikato) for helpful discussions, and to Pat Gread (Waikato) and the technical staff in the Department of Chemistry (NUS) for support services.

References

1 *Transition Metal Sulfur Chemistry: Biological and Industrial Significance*, ed. E. I. Stiefel and K. Matsumoto, American Chemical Society, Washington DC, 1996; J. Wachter, *Angew. Chem., Int. Ed. Engl.*, 1989, **28**, 1613; M. Hidai, S. Kuwata and Y. Mizobe, *Acc. Chem. Res.*, 2000, **33**, 46.
2 D. W. Stephan, *Coord. Chem. Rev.*, 1989, **95**, 41.
3 M. A. Casado, J. J. Pérez-Torrente, M. A. Ciriano, A. J. Edwards, F. J. Lahoz and L. A. Oro, *Organometallics*, 1999, **18**, 5299.
4 S.-W. A. Fong and T. S. A. Hor, *J. Chem. Soc., Dalton Trans.*, 1999, 639.
5 M. Capdevila, Y. Carrasco, W. Clegg, R. A. Coxall, P. González-Duarte, A. Lledós and J. A. Ramirez, *J. Chem. Soc., Dalton Trans.*, 1999, 3103; S. Narayan and V. K. Jain, *Transition Met. Chem.*, 2000, **25**, 400; V. W.-W. Yam, P. K.-Y. Yeung and K.-K. Cheung, *Angew. Chem., Int. Ed. Engl.*, 1996, **35**, 739.
6 H. Liu, C. Jiang, J. S. L. Yeo, K. F. Mok, L. K. Liu, T. S. A. Hor and Y. K. Yan, *J. Organomet. Chem.*, 2000, **595**, 276.
7 A. L. Tan, M. L. Chiew and T. S. A. Hor, *J. Mol. Struct. (Theochem)*, 1997, **393**, 189.
8 S.-W. A. Fong, J. J. Vittal, W. Henderson, T. S. A. Hor, A. G. Oliver and C. E. F. Rickard, *Chem. Commun.*, 2001, 421; S.-W. A. Fong, W. T. Yap, J. J. Vittal, T. S. A. Hor, W. Henderson, A. G. Oliver and C. E. F. Rickard, *J. Chem. Soc., Dalton Trans.*, 2001, 1986.
9 J. S. L. Yeo, J. J. Vittal, W. Henderson and T. S. A. Hor, *J. Chem. Soc., Dalton Trans.*, 2001, 315.
10 See for example W. Henderson and M. Sabat, *Polyhedron*, 1997, **16**, 1663; W. Henderson and B. K. Nicholson, *Polyhedron*, 1996, **15**, 4015.
11 C. M. Bolinger, T. B. Rauchfuss and S. R. Wilson, *J. Am. Chem. Soc.*, 1984, **106**, 7800; C. M. Bolinger, T. D. Weatherill, T. B. Rauchfuss, A. L. Rheingold, C. S. Day and S. R. Wilson, *Inorg. Chem.*, 1986, **25**, 634.
12 K. E. Howard, T. B. Rauchfuss and S. R. Wilson, *Inorg. Chem.*, 1988, **27**, 3561.
13 M. J. Nicol, C. A. Fleming and J. S. Preston, in *Comprehensive Coordination Chemistry*, Ed. in Chief G. Wilkinson, Pergamon Press, Oxford, 1982, ch. 63.
14 H. Liu, A. L. Tan, K. F. Mok, T. C. W. Mak, A. S. Batsanov, J. A. K. Howard and T. S. A. Hor, *J. Am. Chem. Soc.*, 1997, **119**, 11006.
15 M. Zhou, Y. Xu, L.-L. Koh, K. F. Mok, P.-H. Leung and T. S. A. Hor, *Inorg. Chem.*, 1993, **32**, 1875.
16 P. R. Klich, A. T. Daniher, P. R. Challen, D. B. McConville and W. J. Youngs, *Inorg. Chem.*, 1996, **35**, 347.
17 P. M. Veitch, J. R. Allan, A. J. Blake and M. Schröder, *J. Chem. Soc., Dalton Trans.*, 1987, 2853.
18 W. Henderson, A. G. Oliver and C. E. F. Rickard, *Inorg. Chim. Acta*, 2000, **307**, 144.
19 R. D. Fischer and G. R. Sienel, *J. Organomet. Chem.*, 1978, **156**, 383; R. P. Sperline and D. M. Roundhill, *Inorg. Chem.*, 1977, **16**, 2612.
20 A. A. Pinkerton, F.-P. Ahlers, H. F. Griewing and B. Krebs, *Inorg. Chim. Acta*, 1997, **257**, 77.
21 R. Ugo, G. La Monica, S. Cenini, A. Segre and F. Conti, *J. Chem. Soc. A*, 1971, 522.
22 L. J. Arnold, *J. Chem. Educ.*, 1992, **69**, 811.
23 G. M. Sheldrick, SHELXL-97, Program for the Refinement of Crystal Structures, University of Göttingen, Germany, 1997.
24 G. M. Sheldrick, SADABS, Siemens Area Detector Absorption Correction Program, University of Göttingen, Germany, 1996.